Dalton Transactions

PAPER

Cite this: *Dalton Trans.*, 2015, **44**, 10980

Magnetic colloidal superparticles of Co, Mn and Ni ferrite featured with comb-type and/or linear amphiphilic polyelectrolytes; NMR and MRI relaxometry†

Melita Menelaou,[a] Zacharoula Iatridi,[b] Ioannis Tsougos,[c] Katerina Vasiou,[d] Catherine Dendrinou-Samara*[a] and Georgios Bokias*[b]

Received 27th January 2015,
Accepted 5th May 2015

DOI: 10.1039/c5dt00372e

www.rsc.org/dalton

The ability to encapsulate hydrophobic ferrites in colloidal superparticle structures of an a-telechelic hexadecyl-functionalized poly(methacrylic acid) ($C_{16}H_{33}$-PMAA) polymer with a linear architecture was investigated and compared with that of two amphiphilic comb-type water-soluble copolymers, namely, P(ANa-*co*-DAAm) and P(MANa-*co*-DMA), which are comprised of a poly(sodium acrylate) or poly(sodium methacrylate) backbone and pendent dodecyl acrylamide or dodecyl methacrylate chains, respectively. In the case of $C_{16}H_{33}$-PMAA, the pH-sensitive self-assembly behavior, which was studied through Nile Red probing and TEM, was related to its encapsulation properties. Hydrophobic MFe_2O_4 nanoparticles coated with oleylamine (MFe_2O_4@OAm MNPs, where M = Co, Mn, Ni) with a similar shape and size (~9 nm) and magnetization values of 87.4, 63.1 and 55.0 emu g^{-1} for $CoFe_2O_4$@OAm, $MnFe_2O_4$@OAm and $NiFe_2O_4$@OAm, respectively, were successfully encapsulated into the hydrophobic cores of spherical micellar structures formed by the copolymers in an aqueous solution through a solvent mixing procedure. The synthesized magnetic colloidal superparticles fell in the static dephasing regime (SDR). NMR relaxivity measurements of MFe_2O_4@P(ANa-*co*-DAAm), MFe_2O_4@P(MANa-*co*-DMA) and MFe_2O_4@$C_{16}H_{33}$-PMAA at pH = 4.5 and pH = 7 (where M = Co, Mn, Ni) at 11.7 T were recorded and the transverse relaxivity (r_2) (mM^{-1} s^{-1}) was determined. Among all, the $CoFe_2O_4$@polymers demonstrated the highest r_2 relaxivity values, ranging from 61.6 for $CoFe_2O_4$@$C_{16}H_{33}$-PMAA (pH = 7) to 316.0 mM^{-1} s^{-1} for $CoFe_2O_4$@P(ANa-*co*-DAAm). The relaxation efficiency (r_1 and r_2) of $CoFe_2O_4$@P(ANa-*co*-DAAm) was investigated further by magnetic resonance imaging (MRI) at 1.5 T and 3 T and the r_2/r_1 ratios were found to be 16.5 and 18.2, respectively, indicating its potential use as a T_2 contrast agent.

Introduction

Magnetic nanoparticles (MNPs), such as spinel ferrites with the general formula, MFe_2O_4 (where M = Mn, Co, Fe, Ni), have attracted considerable attention due to their composition, size and shape dependent magnetic properties in various fields, ranging from electronics to bioapplications.[1] Although great progress has been done in the past few decades and even iron oxides have been commercialized for medical diagnosis, the successful use of MNPs in biomedical applications is complicated and MNPs are still being developed to enhance the magnetic properties and specificity to biological functions. On this basis, a new family of nanomaterials is generated by clustering small MNPs to larger particles in a colloidal phase, namely, magnetic colloidal superparticles (MSPs).[2] These subsidiary functional materials exhibit collective chemical and physical properties inherited from their constituent nanoparticles and are proposed to overcome the limitations of primary MNPs.[2] For example, cooperative magnetic behavior within highly crystalline iron oxide into raspberry-like or spherical superparticles[2] was found, which can improve the diagnostic effectiveness and/or act as simultaneous therapeutic agents over existing nanostructures while preserving the biocompatibility. Fundamentally, the efficacy of magnetic nanoparticles, either as single particles or superparticles, to act as T_2-contrast agents for Magnetic Resonance Imaging (MRI) is related to the

[a]*Department of Chemistry, Aristotle University of Thessaloniki, GR-54124 Thessaloniki, Greece. E-mail: samkat@chem.auth.gr; Fax: (+30) 2310-997876; Tel: (+30) 2310-997876*
[b]*Department of Chemistry, University of Patras, GR-26504 Patras, Greece. E-mail: bokias@upatras.gr; Fax: (+30) 2610-997122; Tel: (+30) 2610-997102*
[c]*Department of Medical Physics, University Hospital of Larissa, University of Thessaly, Biopolis, GR-41110 Larisa, Greece*
[d]*Department of Radiology, University Hospital of Larissa, University of Thessaly, Biopolis, GR-41110 Larisa, Greece*
†Electronic supplementary information (ESI) available. See DOI: 10.1039/c5dt00372e

transverse relaxivity (r_2), which depends on their size and the square of the saturation magnetization ($R_2 = 1/T_2 \propto \mu^2$).[3] Moreover, the nature of the surface coating around the magnetic core is crucial because it controls the diffusion of water protons and the assembly of magnetic nanoparticles.[4] In fact, three different regimes have been predicted, where such factors can influence the relaxivity and therefore the contrast enhancement: the motional average regime (MAR), the static dephasing regime (SDR) and the echo-limiting regime (ELR).[5]

The preparation of MSPs is based on the colloidal assemblies, arisen through the one step solvothermal route, microwave assisted synthesis or post transformation routes, involving evaporation-induced preparations, offer precise control of the superparticle size.[6] The synthesis of new polymers with specific properties for the encapsulation of MNPs is of great importance nowadays, as the resulted MSPs can improve the targeting efficiency in bioapplications, and be degraded into small particles, which can be subsequently less harmful for the body.[7]

The dispersion of hydrophobic MNPs in water through polymer encapsulation for potential MRI applications is a prerequisite for *in vitro* and *in vivo* applications. This is a major intriguing challenge for us and other groups. Within this context, a variety of amphiphilic diblock copolymers[8–12] as well as alkyl-functionalized comb-type copolymers[13–17] (often called hydrophobically modified water-soluble polymers (HMWSP)) have been explored, where monodispersed or superparticle structures can be formed through hydrophobic interactions and van der Waals forces, depending on the type of grafted tail and the grafting density. For example, the hydrophilization of iron oxide nanoparticles has been applied successfully using poly(maleic anhydride-*alt*-1-octadecene) modified with 5000 Da polyethylene glycol (PEG) or short ethylene glycol (EG) chains.[14] In another study, Peng *et al.*[17] demonstrated the ability of poly(maleic anhydride-*alt*-1-octadecene)-*g*-poly(ethylene glycol) amphiphilic copolymers (PMAO-*g*-PEG) to form water soluble manganese ferrite MSPs. Recently, we demonstrated that solvothermally prepared hydrophobic $CoFe_2O_4$ MNPs coated with oleylamine ($CoFe_2O_4$@OAm) could be encapsulated successfully above the critical micellization concentration (CMC) of the HMWSPs used, to form spherical hydrophilic superparticles.[18] These HMWSPs were comprised of a poly(sodium methacrylate) (PMANa) or poly(sodium acrylate) (PANa) backbone and pendent dodecyl methacrylate (DMA) or dodecyl acrylamide (DAAm) chains. However, to our knowledge, reports on the use of alkyl modified amphiphilic copolymers with a linear architecture for such applications are very rare.[19] Nevertheless, alkyl thiolether end-functionalized polymers, usually bearing poly(acrylic acid) (PAA), poly (methacrylic acid) (PMAA) or poly(vinyl acetate) (PVAc), with 1-dodecane thiol have been recently exploited in the synthesis of size-controlled Au NPs, Co NPs or Fe_3O_4 NPs.[19–23]

Herein, we extend our studies on HMWSPs while we exploit the amphiphilic nature of an alkyl-functionalized copolymer with a linear architecture for the hydrophilization of hydrophobic primary building units, namely, oleylamine-coated MFe_2O_4 (M = Co, Mn, Ni) MNPs of different magnetization values. Thus, an a-telechelic hexadecyl-functionalized poly (methacrylic acid) ($C_{16}H_{33}$-PMAA, see Scheme 1) was tested as potential encapsulating polymeric agent and compared with the comb-type HMWSPs, denoted as P(MANa-*co*-DMA) and P (ANa-*co*-DAAm) (see Scheme 1), respectively. While polymers of different architecture were tested, we chose to keep the size and shape of the primary building units constant because the size and shape of the MNPs have been previously shown to affect the relaxivities; to the best of our knowledge, such comparison is being studied for the first time. In addition, because the (meth)acrylic units are weakly acidic in the case of $C_{16}H_{33}$-PMAA, the pH-sensitive encapsulating ability was explored at both pH = 4.5 and pH = 7. The relaxometric properties of the colloidal superparticles among MFe_2O_4 (M = Co, Mn, Ni) MNPs and the synthesized copolymers have been preevaluated by the NMR relaxivity (r_2) studies, while MRI measurements at 1.5 T and 3 T of the most promising material, namely, $CoFe_2O_4$ MSPs, were taken.

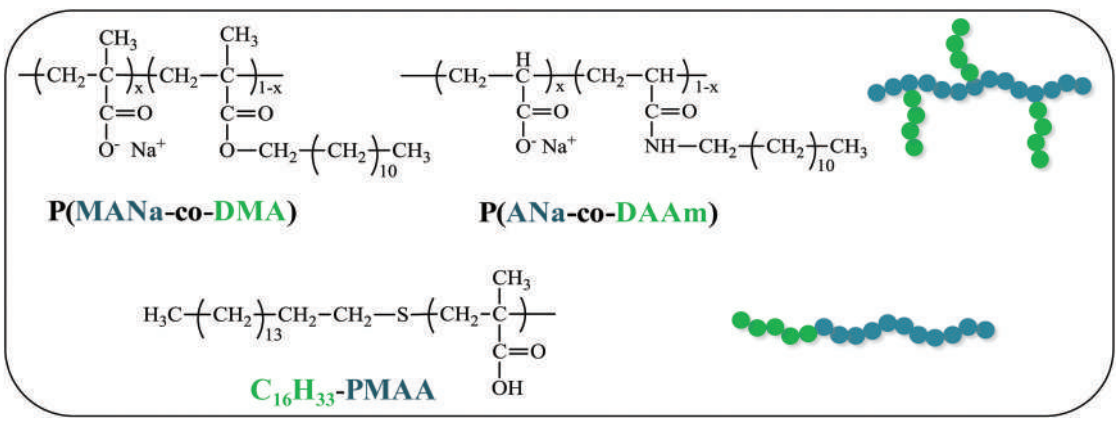

Scheme 1 Chemical structure and schematic depiction of the comb-type and linear architecture of the copolymers used in the present work.

Experimental part

Materials

The monomer methacrylic acid (MAA) and the fluorescent probe Nile Red were purchased from Fluka. 1-Hexadecanethiol was purchased from Alfa Aesar. The initiator azobisisobutyronitrile (AIBN), cobalt(III) acetylacetonate (≥99.9%, $Co(acac)_3$), manganese(III) acetylacetonate (≥99.9%, $Mn(acac)_3$), oleylamine (OAm), diphenyl ether (≥99%, DPHE) and the solvents tetrahydrofuran (THF), dioxane, petroleum ether and deuterated dimethyl sulfoxide (d_6-DMSO) were all purchased from Aldrich. Nickel(II) acetylacetonate (≥99.9%, $Ni(acac)_2$) was supplied by Riedel-de Haën. Ultrapure 3D-water was obtained using a SG Waters apparatus.

Synthesis of α-telechelic hexadecyl-functionalized copolymer ($C_{16}H_{33}$-PMAA)

$C_{16}H_{33}$-PMAA was synthesized by the chain-transfer method utilizing 1-hexadecanethiol as the chain transfer agent. Typically, MAA, 1-hexadecanethiol and AIBN were dissolved in dioxane in a round-bottom flask equipped with a reflux condenser. The reaction mixture was degassed with nitrogen for 2 hours and then left overnight under stirring at 60 °C. The final polymer was recovered through precipitation in petroleum ether and dried under vacuum at 40 °C. After purification, it was characterized by ^{1}H-NMR. The molecular weights and polydispersity were determined by GPC.

Synthesis of comb-type copolymers

The synthesis of the P(MANa-*co*-DMA) and P(ANa-*co*-DAAm) copolymers is described elsewhere.[18] Briefly, P(MANa-*co*-DMA) copolymer was prepared through the free radical copolymerization of methacrylic acid and dodecylmethacrylate in THF at 70 °C, using AIBN as the initiator. This product was transformed to the sodium salt form, P(MANa-*co*-DMA), through neutralization with NaOH and recovered by freeze-drying after purification through dialysis. For the synthesis of P(ANa-*co*-DAAm), PAA (M_W = 5000 g mol^{-1}) was grafted with dodecylamine in DMF at 60 °C, using DCC as the condensing agent. After 24 hours, the solution was vacuum filtered to remove the unwanted dicyclohexyl urea byproduct and finally the sodium salt form was precipitated upon the addition of a certain quantity of 1 M NaOH aqueous solution. The final product was washed with DMF and methanol, vacuum filtered and dried in a vacuum oven at 60 °C.

Solvothermal synthesis of MFe_2O_4@OAm nanoparticles

Based on previous results, MFe_2O_4@OAm MNPs (where M = Co, Mn, Ni) were prepared by solvothermal route.[18,24,25] Briefly, 1.8 mmol of $Fe(acac)_3$ and 0.9 mmol of $M(acac)_2$ (M = Ni)/$M(acac)_3$ (M = Co, Mn) were dissolved either in only OAm (M = Co) or in a mixture of OAm and DPHE (M = Mn, Ni). The resulting solution was stirred thoroughly and then transferred to a 23 mL Teflon-lined stainless-steel autoclave. The autoclave was placed in an electrical oven and the temperature was increased to 200 °C for 24 h. The autoclave was then cooled to room temperature and the resulting product was washed with ethanol; thus, the hydrophobic MFe_2O_4@OAm MNPs were obtained.

Preparation of magnetic colloidal superparticles MFe_2O_4@polymer

Aqueous solutions of P(MANa-*co*-DMA), P(ANa-*co*-DAAm) and $C_{16}H_{33}$-PMAA at specific polymer concentrations were prepared in 3D water and stirred overnight. A small volume of a THF dispersion of $CoFe_2O_4$@OAm, $MnFe_2O_4$@OAm or $NiFe_2O_4$@OAm MNPs was added to the aqueous polymer solutions. The polymer/MNPs mixing ratio was adjusted to 10/1 by weight. The mixtures were sonicated in a Branson 1510 70 W, 40 kHz sonicator and then left at 40 °C until the full evaporation of THF. After THF removal, a fraction of the MNPs precipitated. This fraction was discarded and the supernatant was used for further studies.

Characterization techniques

^{1}H-NMR spectra of the copolymers in d_6-DMSO or D_2O were obtained on a Bruker Advance DPX 400 MHz spectrometer. The acid form of the copolymers, soluble in THF, was used for Gel Permeation Chromatography (GPC) characterization. Two PLgel MiniMix columns "C" and "D" (molecular range 4000–340 000 g mol^{-1}) were used and calibrated with polystyrene standards. THF was used as the eluent. The elution rate was 0.5 mL min^{-1}. Powder X-ray diffraction (XRD) was performed using a 2-cycle Rigaku Ultima + diffractometer (40 kV, 30 mA, CuKa radiation) with Bragg-Brentano geometry (detection limit approximately 2%). The elemental composition of the samples was tested by inductively coupled plasma atomic emission spectroscopy (ICP-AES, Perkin-Elmer Optima 3100XL). Fourier Transform Infrared Spectroscopy was performed on a Nicolet FTIR 6700 spectrometer with KBr pellets in the range of 350–4000 cm^{-1}. Thermogravimetric Analysis (TGA) was performed using SETA-RAM SetSys-1200 and carried out in the range from room temperature to 850 °C at a heating rate of 10 °C min^{-1} under a N_2 atmosphere. Magnetic measurements were performed at 300 K in a 1.2H/CF/HT Oxford Instruments VSM as the function of the applied field (1 T).

Physicochemical characterization. *Nile Red fluorescence probing*. The steady-state fluorescence spectra of Nile Red were recorded on a Perkin Elmer LS50B luminescence spectrometer. A small volume (5 μL) of a stock THF solution, containing 1 × 10^{-3} M Nile Red, was added to 3 mL of an aqueous polymer solution. The final concentration of the probe was fixed at 1.7 × 10^{-6} M. The maximum intensity of the emission peak of Nile Red in the region of 600–650 nm, after excitation at 550 nm, was used to detect the formation of the hydrophobic microdomains. The excitation and emission slits were fixed at 10 nm. *Transmission Electron Microscopy (TEM).* TEM experiments were carried out using a JEM 2100 microscope operating at 200 kV. For the TEM investigation of pure MNPs, diluted THF dispersions were used, whereas aqueous solutions/dispersions were used for the TEM investigation of the pure polymers and

colloidal superparticles. *Dynamic light scattering (DLS) and electrophoresis measurements* were carried out at 25 °C using a NanoZetasizer, Nano ZS Malvern apparatus. The incident light source was a 4 mW He–Ne laser at 633 nm and the intensity of the scattered light was measured at 173°. The mean hydrodynamic diameter was determined from the obtained apparent diffusion coefficient through the Stokes–Einstein equation.

NMR relaxivity measurement. The T_2 relaxation times were measured using a 500-MR NMR Spectrometer (500 MHz, Agilent Technologies) at 25 °C using a Carr–Purcell–Meiboom–Gill (CPMG) pulse sequence. The metal ion concentration (Fe + M^{II}) (M = Co, Mn, Ni) of each aqueous solution was measured by inductively coupled plasma optical emission spectroscopy (ICP-OES). T_2 was measured for a range of concentrations (0.05–0.8 mM) of metal ions (Fe + M^{II}). The initial polymer concentration was in all cases 0.2 wt%. Moreover, care was taken during the dilutions to ensure that the final polymer concentration was well above or close to CMC.

MR relaxivity measurement. The longitudinal (T_1) and transverse (T_2) relaxation times at different concentrations (0.0125–0.8 mM) of the metal ions were performed on two clinical MRI Scanners (a 1.5 T Siemens Aera and a 3 T General Electric Sigma) using a Head/Neck coil. The T_1-weighted images were obtained by an inversion recovery (IR) T_1 pulse sequence with variable inversion values (IR = 25–4000 ms) and an echo time (TE) of 12 ms (1.5 T)/43 ms (3 T). The imaging parameters were as follows: (a) 1.5 T; field of view (FOV) = 250 × 250 mm^2, matrix size (MTX) = 128 × 128, number of axial slices = 1, slice thickness = 20 mm, and number of averages (NEX) = 1 and (b) 3 T; field of view (FOV) = 240 × 240 mm^2, matrix size = 416 × 320, number of axial slices = 1, slice thickness = 4 mm, and number of averages (NEX) = 1. T_2-weighted images were obtained by a multi-echo spin-echo T_2 pulse sequence (5 echoes; 25–50–75–100–125 ms, and static TR (2000 ms) for 1.5 T and 8 echoes; 50, 72, 94, 106, 139, 173, 206, 212 ms, and static TR (1560 ms) for 3 T). The imaging parameters were as follows: (a) 1.5 T; FOV = 250 × 250 mm^2, MTX = 256 × 128, number of axial slices = 1, slice thickness = 5.0 mm, and NEX = 1 and (b) 3 T; FOV = 240 × 240 mm^2, MTX = 416 × 320, number of axial slices = 1, slice thickness = 4.0 mm, and NEX = 1. The resulting set of images was processed offline using an image sequence analysis tool developed in IDL (IDL 8.2, Bolder, USA). T_1 and T_2 analyses were carried out by fitting a monoexponential curve to the image intensities measured on the selected regions of interest (ROIs) for each axial slice.

Results and discussion

In the present study, we used ~9 nm building units of MNPs because it has been shown previously that small sizes (often lower than 7 nm) cannot influence positively the r_2 values, while slightly larger sizes can lead to optimized results.[26] Therefore, we adopted a previously reported solvothermal synthesis to isolate ferrite MNPs with a similar size and shape.[18,24,25] In brief, fine cubic spinel structures *Fd3m* of ferrite nanoparticles, MFe_2O_4 (where M = Co, Mn, Ni), were synthesized solvothermally using metal acetylacetonates precursors in the presence of oleylamine (OAm). The crystal structures of the primary units were verified by XRD (Fig. S1a†), while the crystallite sizes were calculated using Scherrer's formula at 9.2 nm for $CoFe_2O_4$@OAm, 9.0 nm for $MnFe_2O_4$@OAm and 9.3 nm for $NiFe_2O_4$@OAm, respectively; almost identical sizes compared to those found by TEM images were observed (Fig. 1a–c). The presence of OAm was certified by FT-IR spectroscopy (Fig. S1b†) and the total weight loss was determined by thermogravimetric analysis (TGA), which is equal to 27.5 wt%, 23.0 wt% and 29.5 wt% for $CoFe_2O_4$@OAm, $MnFe_2O_4$@OAm and $NiFe_2O_4$@OAm (Fig. S1b and c†). In addition, using the TGA results, the coverage of OAm molecules surrounding each nanoparticle was quantified. Based on the assumption that all nanoparticles are spherical, the number of OAm ligands (N) for each MFe_2O_4 system was calculated using eqn (1);[27] 1338.2 ($CoFe_2O_4$@OAm NPs), 1029.2 ($MnFe_2O_4$@OAm MNPs) and ~1352.5 ($NiFe_2O_4$@OAm NPs), respectively. In addition, based on eqn (1),[27] the number of molecules per area ($A = 4\pi R^2$) was calculated; 5.03×10^{14} ($CoFe_2O_4$@OAm MNPs), 4.04×10^{14} ($MnFe_2O_4$@OAm MNPs) and 5.20×10^{14} ($NiFe_2O_4$@OAm MNPs). These results can further provide stronger evidence of the thickness of the organic coating around the metal core for each of the three systems studied.

$$N = \frac{\omega N_A \rho \frac{4}{3}\pi R^3 10^{-23}}{MM} \quad (1)$$

where N is the number of ligands on each particle, R is the mean radius of the MFe_2O_4 NPs, ρ is the density of the MFe_2O_4 MNPs (M = Co, Mn, Ni; 5.304 g cm^{-3}, 5.21 g cm^{-3} and 5.164 g cm^{-3}, respectively), N_A is Avogadro's number, MM is the mean molar mass of the OAm molecules (g mol^{-1}), and ω is the mass loss (%).

The resulting ferrite MNPs displayed enhanced M_s values depending on the nature of the divalent ion with absolute magnetization values at 87.4 emu g^{-1} for $CoFe_2O_4$@OAm, 63.1 emu g^{-1} for $MnFe_2O_4$@OAm and 55.0 emu g^{-1} for $NiFe_2O_4$@OAm (Fig. S1d†).

Formation of magnetic colloidal superparticles with comb-type copolymers

For the formation of colloidal superparticles of MFe_2O_4@OAm (M = Co, Mn, Ni) MNPs, two comb-type HMWSPs based on a carboxylate backbone and dodecyl- side chains, namely, P(MANa-*co*-DMA) and P(ANa-*co*-DAAm), were explored. The chemical structure and the depiction of the architecture of the comb-type copolymers are shown in Scheme 1, while the characterization results of the copolymers are tabulated in Table 1.[18] In our previous report, $CoFe_2O_4$@HMWSPs nanohybrids were effectively stabilized in water through a solvent mixing procedure.[18] In the present work we further extend this concept and utilize comb-type copolymers to disperse hydrophobic $MnFe_2O_4$@OAm and $NiFe_2O_4$@OAm MNPs.

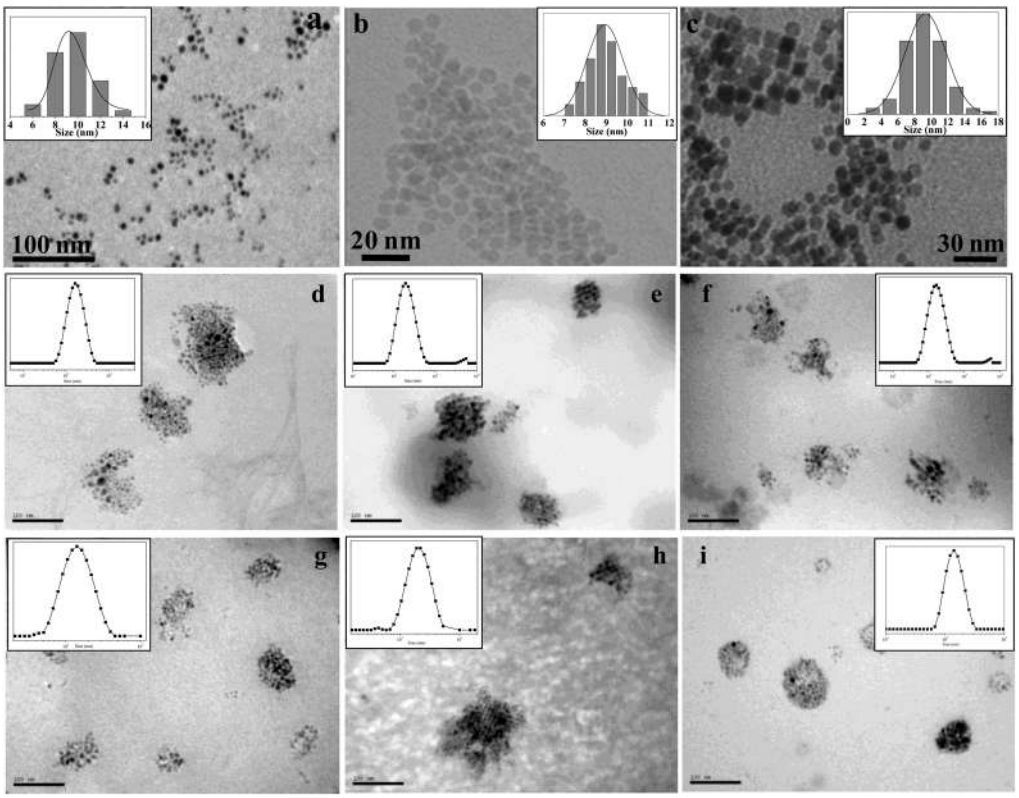

Fig. 1 TEM images of single particles (a) $CoFe_2O_4$@OAm, (b) $MnFe_2O_4$@OAm and (c) $NiFe_2O_4$@OAm as well as MFe_2O_4@P(MANa-co-DMA), where (d) M = Mn, (e) M = Ni, (f) M = Co, and MFe_2O_4@P(ANa-*co*-DAAm), where (g) M = Mn, (h) M = Ni and (i) M = Co. The copolymer concentration is 0.3 wt% (above CMC for both polymers). Scale bar in (d)–(i): 100 nm. Inset: distribution of the hydrodynamic diameter as determined by DLS.

Table 1 Physicochemical characterization of the amphiphilic copolymers

Copolymer	Composition (^{1}H-NMR)[b]	M_n, g mol^{-1} (GPC)	M_w, g mol^{-1} (GPC)	ζ-Potential, mV	CMC[d], wt%
P(MANa-*co*-DMA)[a]	75	27 800	73 600	−40.7	0.002
P(ANa-*co*-DAAm)[a]	90	—	7500[c]	−46.8	0.100
$C_{16}H_{33}$-PMAA	94	2600	3600	−15.9 (at pH 7.5)	0.020
				−10.0 (at pH 4.5)	0.002

[a] From ref. 18. [b] % Moles of MANa, ANa or MAA units. [c] Calculated from the nominal mass of PAA and the composition of the copolymer, as found by ^{1}H-NMR. [d] From Nile Red probing.

Representative TEM images of the spherical nanostructures stabilized in water, and the intensity-weighted distribution of the hydrodynamic diameter (determined through DLS) of MFe_2O_4@P(MANa-*co*-DMA) and MFe_2O_4@P(ANa-*co*-DAAm) (where M = Mn, Ni, Co) are shown in Fig. 1. The hydrodynamic diameter was ~180 nm and ~140 nm for $MnFe_2O_4$@P(MANa-*co*-DMA) (inset of Fig. 1d) and $MnFe_2O_4$@P(ANa-*co*-DAAm) (inset of Fig. 1g), respectively. The estimated diameter from TEM images varied in the range of 90–100 nm (Fig. 1d) and 45–65 nm (Fig. 1g) for the $MnFe_2O_4$@P(MANa-*co*-DMA) and $MnFe_2O_4$@P(ANa-*co*-DAAm) nanohybrids, respectively. A similar behavior was exhibited by the $NiFe_2O_4$@copolymer samples; $NiFe_2O_4$@P(MANa-*co*-DMA) nanohybrids form nanostructures (Fig. 1e) with a diameter of ~180 nm (from DLS) and 70–90 nm (from TEM), while $NiFe_2O_4$@P(ANa-*co*-DAAm) form nanostructures (Fig. 1h) with a diameter of ~185 nm (from DLS) and 150–170 nm (from TEM). Finally, the size of the $CoFe_2O_4$@P(MANa-*co*-DMA) was ~150 nm (from DLS) and 65–90 nm (from TEM) (Fig. 1f) and ~140 nm (from DLS) and 45–90 nm (from TEM) for $CoFe_2O_4$@P(ANa-*co*-DAAm) (Fig. 1i). Although there are no such large numerical differences in the organic coating of the primary building MNPs, taking the similar sizes of the metal core and the same surfactant into account, we assume that the way of bounding and/or small differences of the thickness of the organic coating influences the uniform supramolecular structures formation.

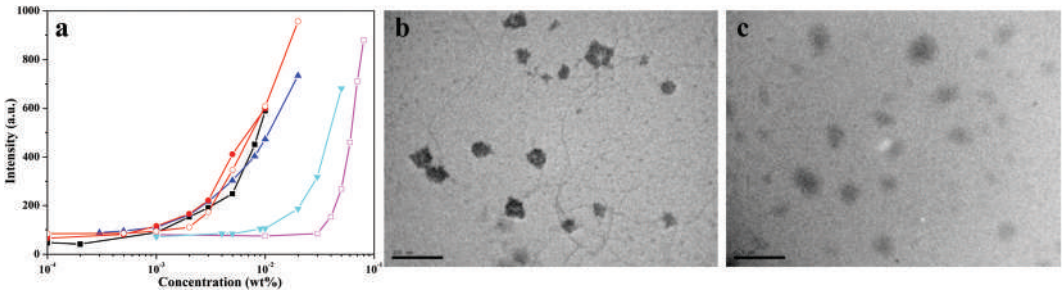

Fig. 2 (a) Dependence of the maximum fluorescence intensity of Nile Red at 600–650 nm on the $C_{16}H_{33}$-PMAA concentration in buffer solutions (pH = 2 (■), pH = 4.5 (●), pH = 5.5 (▲), pH = 6 (▼) and pH = 7 (□) or at pure water (pH = ~4.5) (○)), TEM images of aqueous $C_{16}H_{33}$-PMAA solutions at (b) 0.01 wt% and pH = 4.5 (above CMC, scale bar: 100 nm) and (c) 0.3 wt% and pH = 7.5 (above CMC, scale bar: 500 nm).

Formation of magnetic colloidal superparticles (MSPs) with the linear copolymer $C_{16}H_{33}$-PMAA

Synthesis and characterization of linear polymer $C_{16}H_{33}$-PMAA. Thiol-containing molecules are efficient chain transfer agents and, in combination with adequate initiators like azobisisobutyronitrile (AIBN)[19–23] or ammonium persulfate,[28] they are applied for chain transfer polymerizations in organic or aqueous media, respectively. As a consequence of the chain transfer polymerization mechanism, the thiol group is attached to one end of the polymer chain, through a thioether bond, leading to products of low molecular weights and narrow polydispersity.[22] The synthesis of functional thioether polymers using monomers like acrylic acid (AA) or methacrylic acid (MAA) and dodecanethiol as chain transfer agent has already been reported.[19–23] Herein, we apply this methodology for the synthesis of an α-telechelic amphiphilic copolymer, namely poly(methacrylic acid), PMAA, end-functionalized with a more hydrophobic, longer alkylthiol, namely 1-hexadecanethiol. Dioxane was chosen as a desirable reaction solvent for the monomer MAA, the chain transfer agent 1-hexadecanethiol and the initiator AIBN. The chemical structure and schematic depiction of the architecture of $C_{16}H_{33}$-PMAA are shown in Scheme 1. The copolymer was characterized by ^{1}H-NMR using d_6-DMSO as a deuterated solvent, and GPC in THF. The characterization results are summarized in Table 1. From the ^{1}H-NMR characterization, the MAA content of the copolymer was found to be 94 mol%. This suggests that ~16 MAA units are polymerized at each hexadecanethiol group, leading to an estimated number-average molecular weight, $M_n \sim 1630$ g mol^{-1}. This value is in good agreement with the value $M_n = 2600$ g mol^{-1} determined by GPC, using polystyrene standards. Moreover, from GPC characterization, the weight-average molecular weight, M_w, is determined to be $M_w = 3600$ g mol^{-1}. Therefore, the obtained low molecular weight together with the observed narrow polydispersity index (PI = 1.38) suggests that a chain transfer polymerization mechanism is indeed effective.

Because the PMAA block of $C_{16}H_{33}$-PMAA is a weak polyacid, *i.e.* the degree of dissociation depends on the pH of the solution, this copolymer is expected to exhibit pH-sensitive self-association behavior in aqueous media. In fact, this is shown in Fig. 2a, where the influence of pH on the CMC of $C_{16}H_{33}$-PMAA is investigated in aqueous buffer solutions ($4.5 < pH < 7$) through fluorescence probing with Nile Red. Nile Red is poorly soluble in water but its solubility increases in a less polar environment. In addition, it is almost non-fluorescent in water and other polar solvents, while it is strongly fluorescent in less polar environments, showing an intense emission peak in the region, 600–650 nm. The CMC is the polymer concentration, above which the amphiphilic copolymers form micellar-like structures with hydrophobic cores consisting of the pendant alkyl chains and hydrophilic coronas consisting of anionic polyelectrolyte backbones. As can be observed, the copolymer exhibits similar behavior in all buffer solutions for $pH \leq 5.5$. Within this pH region, the PMAA block is just slightly ionized, as suggested by the low absolute ζ-potential value (Table 1) of the formed micellar aggregates because the pK_a of pure PMAA is estimated to be p$K_a \sim 5.5$.[29] As a result, the CMC of the copolymer, which is determined as the polymer concentration at the onset of the fluorescence intensity of the probe, is ~0.001 wt% for $pH \leq 5.5$. For pH higher than the pK_a of pure PMAA, the carboxylic groups of PMAA block become gradually ionized, the polyacid blocks were more extended and a higher polymer concentration is necessary to detect micellar nanostructures in aqueous media. Thus, the CMC is detected at a polymer concentration of 0.01 and 0.03 wt% for the buffer solutions with pH = 6 and pH = 7, respectively, while the formed micellar aggregates are characterized by a higher absolute ζ-potential value (Table 1). Finally, when the copolymer was dissolved in pure water, the solution was slightly acidic, pH = ~4.5, as expected. However, compared to the behavior observed in the buffer solution with pH = 4.5, the CMC of the copolymer in pure water was higher, CMC ~ 0.002 wt%. This slight CMC difference was attributed to the presence of a salt in the buffer solution, enabling self-association, as a consequence of the screening of the (low) fraction of charges along the polyacid block.

To obtain visual confirmation of the nanostructures formed by the $C_{16}H_{33}$-PMAA copolymer in aqueous media, TEM characterization was performed at polymer concentrations above CMC and at two pH values, pH = 4.5 and pH = 7.5.

Representative results are shown in Fig. 2. The size of the aggregates formed at lower pH values is generally smaller than that of the aggregates formed at a more basic environment. More specifically, the copolymer forms micellar nanostructures with a diameter of 25–50 nm at pH = 4.5 (Fig. 2b) and 125–325 nm at pH = 7.5 (Fig. 2c). The formed micelles at pH = 4.5 are probably multichain aggregates with a spherical shape where the hydrophobic hexadecane units are located in the center, while the hydrophilic PMAA blocks provide water solubility and stability of the formed micelles in the aqueous solution. When the pH was increased to higher values, the aggregates formed displayed an expansion in size, due to the enhanced osmotic pressure of the counter-ions trapped inside the polymeric network by the electrostatic attraction exerted by the charged carboxylate groups.[29,30] As a consequence, the multichain aggregates formed at low pH probably change to large-compound micelles at pH = 7.5. This has been shown in the case of amphiphilic P(MANa-*co*-DMA) and P(ANa-*co*-DAAm) comb-type copolymers.[18]

Encapsulation of hydrophobic MNPs by the linear $C_{16}H_{33}$-PMAA copolymer. End-telomerized polymers with dodecyl groups have previously been reported to disperse Au NPs, Co NPs or iron oxide NPs in aqueous media.[19–23] In all cases, the nanoparticles were *in situ* synthesized, using either reduction agents or basic solutions in the presence of the polymer. In contrast, in the present study, a post synthetic procedure was applied to form the colloidal superparticles between the already prepared hydrophobic MNPs, taking advantage of the ability of the polymer to form water soluble micellar-type structures. Representative TEM images and the distribution of the hydrodynamic diameter measured by DLS of the colloidal superparticles (MFe_2O_4@$C_{16}H_{33}$-PMAA (M = Co, Mn, Ni)) are shown in Fig. 3. The assemblies formed are generally observed to be smaller in TEM with respect to the DLS results, due to the solvent evaporation and shrinkage or dehydration of the micellar aggregates. In the TEM images, only the hydrophobic cores with the incorporated MFe_2O_4@OAm MNPs are observable and not the hydrophilic part of the micelles due to the high contrast of the MNPs. Therefore, although similar hydrodynamic sizes of ~125–160 nm were found by DLS, from the TEM investigation, the importance of pH and/or the nature of MNPs is evidenced more clearly. The supramolecular structures formed by the MFe_2O_4@$C_{16}H_{33}$-PMAA appear to be more uniform in the case of the Co and Mn ferrite MNPs while in the case of Ni, they are less uniform, possibly due to dispersibility limitations. The mean size of the aggregates appears to increase with pH, which is in qualitative agreement with the behavior of the pure copolymer above the CMC (Fig. 2). This is clearer in the case of $CoFe_2O_4$@$C_{16}H_{33}$-PMAA (the mean size increases from ~40–60 nm at pH = 4.5 to 100–120 nm at pH = 7.5) and $NiFe_2O_4$@$C_{16}H_{33}$-PMAA (at pH = 4.5 the smaller objects with sizes of ~30–40 nm appear to disappear and be replaced by objects with a more uniform size of ~90–100 nm at pH = 7.5). In addition, the uniformity at the same pH between the different MNPs can be explained, as stated before, by the organic coating of the primary building MNPs.

Based on the hydrodynamic diameters of the MSPs formed either by the linear or the two comb-type amphiphilic copolymers, the maximum number of single nanoparticles in a superparticle (N_{Sup}) was calculated using eqn (2).[5] The results are listed in Table 2; roughly ~15–20 MNPs may fit in one MSP for all systems.

$$\frac{4}{3}\pi {R_{Sup}}^3 = N_{Sup}\frac{4}{3}\pi R^3 \quad (2)$$

where R_{Sup} is the superparticle radius (determined by DLS), R is the radius of the nanoparticle, and N_{Sup} is the number of nanoparticles in the superparticle.

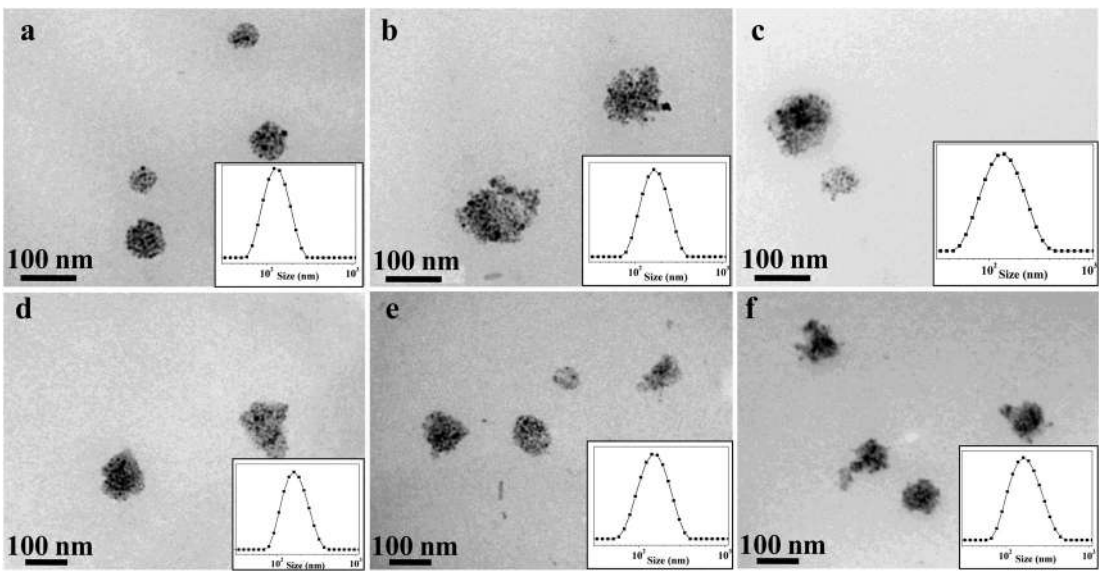

Fig. 3 TEM images of MFe_2O_4@$C_{16}H_{33}$-PMAA, where (a and d) M = Co, (b and e) M = Mn and (c and f) M = Ni above CMC (0.3 wt%) at pH = 4.5 (a, b, c) and pH = 7.5 (d, e, f). Scale bar: 100 nm. Inset: distribution of the hydrodynamic diameter, as determined by DLS.

Table 2 D_{hydro}: the hydrodynamic diameter (DLS) of the superparticles, N_{Sup}: number of single nanoparticles in the superparticle; ζ-potential; Δ_ω: the Larmor frequency shift; τ_D: the translational time and r_2: relaxivity values of the MSPs in the presence of the copolymers

Polymer employed in the encapsulation process	D_{hydro} (nm)	N_{Sup}	ζ-Potential (mV)	$\Delta_\omega\tau_D$	r_2 (mM^{-1} s^{-1})	Regime
$CoFe_2O_4$@OAm/9.2 nm/87.4 emu g^{-1}						
P(ANa-*co*-DAAm)	140	16	−57.1	12.5	316.0	SDR[a]
P(MANa-*co*-DMA)	150	17	−45.7	15.2	210.7	SDR
$C_{16}H_{33}$-PMAA (pH = 4.5)	125	14	−23.8	10.3	180.3	SDR
$C_{16}H_{33}$-PMAA (pH = 7)	160	18	−58.7	17.5	61.60	SDR
$MnFe_2O_4$@OAm/9.0 nm/63.1 emu g^{-1}						
P(ANa-*co*-DAAm)	130	14	−43.3	8.30	128.7	SDR/MAR[b]
P(MANa-*co*-DMA)	180	20	−35.9	16.6	152.5	SDR
$C_{16}H_{33}$-PMAA (pH = 4.5)	160	18	−21.0	12.9	75.90	SDR
$C_{16}H_{33}$-PMAA (pH = 7)	140	16	−54.7	10.0	49.90	SDR
$NiFe_2O_4$@OAm/9.1 nm/55.0 emu g^{-1}						
P(ANa-*co*-DAAm)	185	21	−42.2	13.9	110.4	SDR
P(MANa-*co*-DMA)	180	20	−35.6	13.0	95.90	SDR
$C_{16}H_{33}$-PMAA (pH = 4.5)	125	14	−21.6	6.50	51.20	SDR
$C_{16}H_{33}$-PMAA (pH = 7)	160	18	−57.3	10.8	37.30	SDR

[a] SDR: static dephasing regime. [b] MAR: motional average regime.

NMR and MR relaxivity measurements

The efficiency of magnetic nanoparticles to act as T_2-contrast agents for MRI is related to the transverse relaxivity (r_2), which occurs in three different regions while theoretical models have been described to predict relaxivity in each regime.[31] In the first regime, which is called the motional average regime (MAR) or outer sphere, r_2 increases with the size of the MSPs, while in the second regime, called the static dephasing regime (SDR), which is the most interesting from the MRI point of view, the highest relaxivities occur and depend on the magnetization properties of the MSPs and not on the shape or density of the MSPs.[31] In the third regime, called the echo-limiting regime (ELR), an echo-dependent decrease of relaxation is observed and is expected to be independent of the shape of the MSPs.[31]

The size dependence of the r_2 in MAR originates from the diffusion of water molecules and the regime is reached only when the Redfield condition is fulfilled ($\gamma B_{eq}\tau_D < 1$ or $\Delta_\omega\tau_D < 1$);[1,31] thus the condition can be expressed by calculating the diffusion time (τ_D) and the equatorial magnetic field (B_{eq}) (eqn (3)). At a certain size, r_2 no longer increases with increasing size, because the SDR is reached ($\gamma B_{eq}\tau_D \gg 1$ or more precisely $5 < \Delta_\omega\tau_D < 20$).[1,31]

$$\tau_D = \frac{d^2}{4D}\ B_{eq} = \frac{\mu_o}{3} M_s\ \Delta_\omega = \gamma B_{eq} \qquad (3)$$

where τ_D is the diffusion time, d is the hydrodynamic diameter (determined by DLS) and D is the water diffusion coefficient ($D = 3 \times 10^{-9}$ m^2 s^{-1}); B_{eq} is the equatorial magnetic field of the MNPs, μ_o is the vacuum magnetic permeability ($4\pi \times 10^{-4}$ T emu^{-1} cm^{-3}), M_s is the normalized magnetization of the MNPs; Δ_ω is the Larmor frequency shift and γ is the proton gyromagnetic ratio.

When the SDR is reached, the transverse relaxation rate, R_2 and R_2^*, are equal and given by[1]

$$R_2^* = \frac{1}{T_2^*} = \frac{2\pi}{3\sqrt{3}}\nu\gamma B_{eq} = \frac{2\pi}{3\sqrt{3}} f\Delta\omega \approx R_2$$

In this respect, at first we examined in which regime the synthesized superparticles fall; $\Delta_\omega\tau_D$ was calculated for all formed MSPs. The values for all the systems were in the range of 6.5 to 17.5, as depicted in Table 2 and SDR regime identified. A linear concentration dependence of the transverse relaxation rate [$R_2(1/T_2)$] with respect to the metal ion concentration (C) was observed by NMR relaxometric measurements for all samples, permitting the determination of transverse relaxivity (r_2) value based on eqn (4) (Fig. 4).[32] The calculated r_2 values are listed in Table 2.

$$R_2 = \frac{1}{T_2} = \frac{1}{T_2^0} + r_2 C \qquad (4)$$

where T_2 is the proton relaxation time in the presence of MNPs, T_2^0 is the proton relaxation time of pure water and C is the concentration of the metal ions (Fe + M^{II}).

The results depicted in Fig. 4 highlight the importance of the difference in the magnetic properties (M_s) of the single ferrite particles ($M_{s\ Co} > M_{s\ Mn} > M_{s\ Ni}$) as well as the difference in the architecture of the amphiphilic polymers (comb-type and linear); the highest r_2 values among the synthesized colloidal superparticles of all samples were obtained when $CoFe_2O_4$ MNPs were used as single particles attributed to the collective magnetic properties of the building units. Moreover, the encapsulation of the single particles in the copolymers with a comb-type architecture featured higher r_2 values for all systems compared to the one with linear architecture (Fig. 5); particularly the highest r_2 value was obtained for $CoFe_2O_4$ and $NiFe_2O_4$ MSPs in the presence of P(ANa-*co*-DAAm) (316.0 mM^{-1} s^{-1} and 110.4 mM^{-1} s^{-1}, respectively). However,

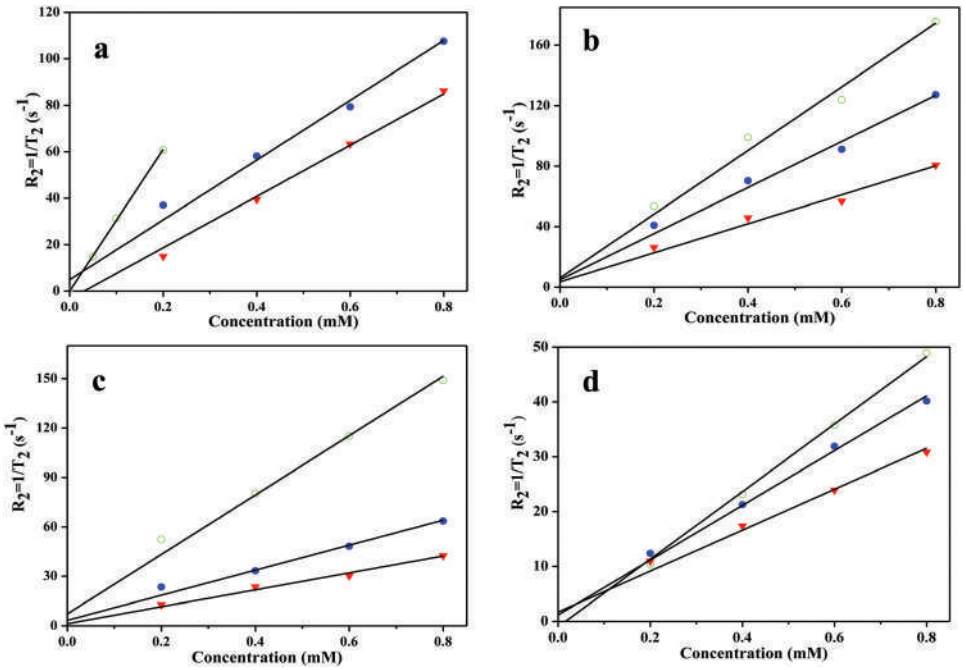

Fig. 4 NMR relaxometric properties of (a) MFe_2O_4@P(ANa-*co*-DAAm), (b) MFe_2O_4@P(MANa-*co*-DMA), (c) MFe_2O_4@$C_{16}H_{33}$-PMAA at pH = 4.5 and (d) MFe_2O_4@$C_{16}H_{33}$-PMAA at pH = 7, where M = Co (○), Mn (●) and Ni (▼), respectively.

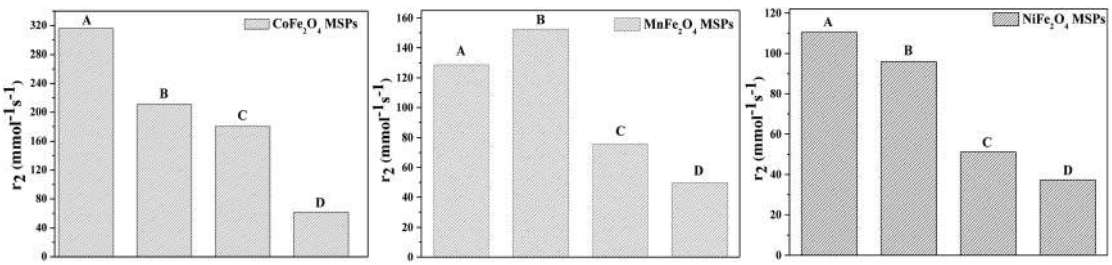

Fig. 5 Transverse relaxivity (r_2) values of Co, Mn, and Ni ferrite MCSs (where: A: P(ANa-*co*-DAAm); B: P(MANa-*co*-DMA); C: $C_{16}H_{33}$-PMAA at pH = 4.5 and D: $C_{16}H_{33}$-PMAA at pH = 7).

the presence of P(ANa-*co*-DAAm) for $MnFe_2O_4$ MSPs, led to lower r_2 value (128.9 mM^{-1} s^{-1}). In this case, the $\Delta_\omega\tau_D$ value is at ~8, which is close to the lower limit of the regime. Therefore, we can assume that $MnFe_2O_4$@P(ANa-*co*-DAAm) is neither in the MAR nor completely in the SDR regime as was previously found.[1] Nevertheless, the highest relaxivity was shown by the comb-type polymer $MnFe_2O_4$@P(MANa-*co*-DMA) (152.5 mM^{-1} s^{-1}). In the case of the linear polymer, the pH values also affected the resulted relaxivities since at pH = 4.5 all MSPs showed increased values compared to those found at pH = 7, which is indicative of the pH dependence (Table 2). Based on the above results, the difference in the architecture of the polymers was proven to be a crucial factor for differentiating the r_2 values of the MSPs. In addition to the different topology, the relatively higher hydrophobic content and higher molecular weight (Table 1) also favor the encapsulation efficiency of the comb-type copolymers compared to that of the linear one. To fully elucidate this behavior, further information is needed regarding the relationship between the encapsulation ability with the polymer architecture (comb-type or linear one), the hydrophilic–lipophilic balance of the copolymers and the respective variation of the aggregation numbers of the resulting polymeric micelles.

Furthermore, the performance of the $CoFe_2O_4$@P(ANa-*co*-DAAm), which exhibited the highest r_2 value, was examined using 1.5 T and 3 T MRI scanners to explore the effectiveness of the system under different magnetic fields. The MR T_1-weighted and T_2-weighted phantom images in Fig. 6 demonstrated the concentration-dependent T_1 brightening effect and T_2 darkening effect. The relaxivity values (r_1 and r_2) were determined by curve fitting of the linear relationship according to eqn (4) (Fig. 6). r_1 and r_2 were found to be 0.58 (1.5 T)/0.7 (3 T) and 9.6 (1.5 T)/12.7 (3 T), respectively. These values were lower than those of the commercially available contrasts agents,

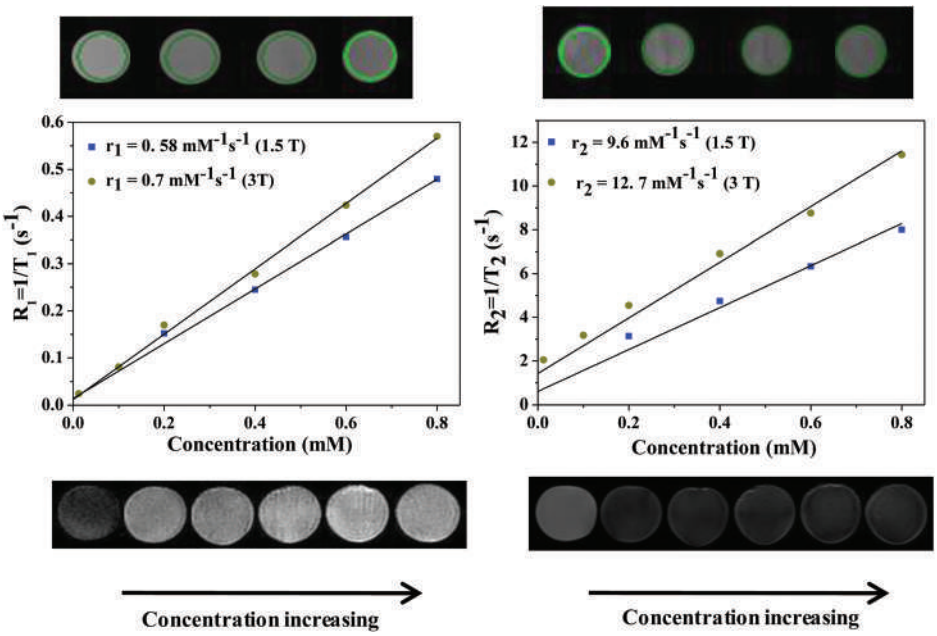

Fig. 6 T_1-weighted and T_2-weighted MR images as well as T_1 and T_2 relaxivity plots of $CoFe_2O_4$@P(ANa-*co*-DAAm) at 1.5 T (■) and 3 T (●), respectively.

such as Magnevist (3.3 (1.5 T)/3.1 (3 T) and 3.9 (1.5 T)/3. 7 (3 T)), Resovist (8.7 (1.5 T)/4.1 (3 T) and 61 (1.5 T)/143 (3 T)) and Feridex (4.6 (1.5 T)/4.1 (3 T) and 41 (1.5 T)/93 (3 T))[33] which can be attributed to various factors including the different structure of the surface coating and the hydrodynamic diameter. However, the r_2/r_1 ratio, which is very important for determining if a contrast agent has mainly a T_1-reducing or T_2-reducing effect, was found to be 16.5 at 1.5 T and 18.2 at 3 T. These values are close to previous reports for the iron oxide MNPs – Feridex/Endorem (8.9 at 1.5 T and 22.7 at 3 T).[33]

Conclusions

Hydrophobically-modified magnetic superparticles (MSPs) can be challenging candidates for biomedical applications including magnetic resonance imaging (MRI). Polymer addition led to controlled clustering and water dispersity, while successful encapsulation can be considered as a host–guest process. The architecture of amphiphilic polymers was found to be crucial to the relaxivity properties of MSPs. Thus, among the polymers tested for the encapsulation of the same primary building blocks of MFe_2O_4@OAm MNPs (M = Co, Mn, Ni), comb-type copolymers exhibit higher r_2 relaxivity values than the linear one. The importance of pH on the relaxivity properties was evaluated using the MSPs formed by the linear copolymer. However, the collective magnetic properties were based on the magnetization of the primary building nanoparticles because a linear correlation with the r_2 relaxivity was found in all cases (Co > Mn > Ni). $CoFe_2O_4$@P(ANa-*co*-DAAm), with the highest NMR r_2 value (316.0 mm^{-1} s^{-1}), exhibited a signal decrease because the MRI T_2-contrast agent with a r_2/r_1 ratio (18.2 at 3 T) was in a similar range to that of a commercially available T_2-contrast agent. The assembly of small particles into a larger particle with a good response to a magnetic field provides further options for specific targeting in bioapplications because of their differentiated accumulation and disassembly in the body.

Acknowledgements

This research was co-financed by the European Union (European Social Fund-ESF) and Greek national funds through the Operational Program "Education and Lifelong Learning" of the National Strategic Reference Framework (NSRF)-Research Funding Program: THALES. Investing in knowledge society through the European Social Fund. The authors thank the Royal Marsden NHS Foundation Trust for the 1.5 T MRI measurements as well as Dr Maria Kollia and Mr Vasilis Kotsopoulos from the Lab of Electron Microscopy and Microanalysis at the University of Patras for the TEM images.

References

1 Q. L. Vuong, J.-F. Berret, J. Fresnais, Y. Gossuin and O. Sandre, *Adv. Healthcare Mater.*, 2012, **1**, 502–512.
2 T. Wang, X. Wang, D. LaMontagne, Z. Wang, Z. Wang and Y. C. Cao, *J. Am. Chem. Soc.*, 2012, **134**, 18225–18228.
3 A. Kostopoulou, S. K. P. Velu, K. Thangavel, F. Orsini, K. Brintakis, S. Psycharakis, A. Ranella, L. Bordonali,

A. Lappas and A. Lascialfari, *Dalton Trans.*, 2014, **43**, 8395–8404.
4 Y. Hu, L. Meng, L. Niu and Q. Lu, *Langmuir*, 2013, **29**, 9156–9163.
5 A. Roch, Y. Gossuin, R. N. Muller and P. Gillis, *J. Magn. Magn. Mater.*, 2005, **293**, 532–539.
6 J. Guo, W. Yang and C. Wang, *Adv. Mater.*, 2013, **25**, 5196–5214.
7 T. Sun, Y. S. Zhang, B. Pang, D. C. Hyun, M. Yang and Y. Xia, *Angew. Chem., Int. Ed.*, 2014, **53**, 12320–12364.
8 B.-S. Kim, J.-M. Qiu, J.-P. Wang and T. A. Taton, *Nano Lett.*, 2005, **5**, 1987–1991.
9 S. Lecommandoux, O. Sandre, F. Checot and R. Perzynski, *Prog. Solid State Chem.*, 2006, **34**, 171–179.
10 A. Bakandritsos, G. Mattheolabakis, R. Zboril, N. Bouropoulos, J. Tucek, D. G. Fatouros and K. Avgoustakis, *Nanoscale*, 2010, **2**, 564–572.
11 A. M. Budgin, Y. A. Kabachii, Z. B. Shifrina, P. M. Valetsky, S. S. Kochev, B. D. Stein, A. Malyutin and L. M. Bronstein, *Langmuir*, 2012, **28**, 4142–4151.
12 S. Mahajan, V. Koul, V. Choudhary, G. Shishodia and A. C. Bharti, *Nanotechnology*, 2013, **24**, 015603.
13 E. V. Shtykova, X. Huang, X. Gao, J. C. Dyke, A. L. Schmucker, B. Dragnea, N. Remmes, D. V. Baxter, B. Stein, P. V. Konarev, D. I. Svergun and L. M. Bronstein, *J. Phys. Chem. C*, 2008, **112**, 16809–16817.
14 E. V. Shtykova, A. Malyutin, J. Dyke, B. Stein, P. V. Konarev, B. Dragnea, D. I. Svergun and L. M. Bronstein, *J. Phys. Chem. C*, 2010, **114**, 21908–21913.
15 Y. Ning, H. Zhang, J. Han, C. Yang, Y. Liu, D. Zhou and B. Yang, *J. Mater. Chem.*, 2011, **21**, 6837–6843.
16 X. Li, H. Li, G. Liu, Z. Deng, S. Wu, P. Li, Z. Xu, H. Xu and P. K. Chu, *Biomaterials*, 2012, **33**, 3013–3024.
17 E. Peng, E. S. G. Choo, Y. Sheng and J. M. Xue, *New J. Chem.*, 2013, **37**, 2051–2060.
18 Z. Iatridi, V. Georgiadou, M. Menelaou, C. Dendrinou-Samara and G. Bokias, *Dalton Trans.*, 2014, **43**, 8633–8643.
19 M. I. Majeed, Q. Lu, W. Yan, Z. Li, I. Hussain, M. N. Tahir, W. Tremel and B. Tan, *J. Mater. Chem. B*, 2013, **1**, 2874–2884.
20 S. Graham, P. A. G. Cormack and D. C. Sherrington, *Macromolecules*, 2005, **38**, 86–90.
21 X. Huang, B. Li, H. Zhang, I. Hussain, L. Liang and B. Tan, *Nanoscale*, 2011, **3**, 1600–1607.
22 L. Zhu, D. Xue and Z. Wang, *Langmuir*, 2008, **24**, 11385–11389.
23 L. T. Lu, L. D. Tung, I. Robinson, D. Ung, B. Tan, J. Long, A. I. Cooper, D. G. Fernig and N. T. K. Thanh, *J. Mater. Chem.*, 2008, **18**, 2453–2458.
24 M. Menelaou, K. Georgoula, K. Simeonidis and C. Dendrinou-Samara, *Dalton Trans.*, 2014, **43**, 3626–3636.
25 K. Vamvakidis, M. Katsikini, D. Sakellari, E. C. Paloura, O. Kalogirou and C. Dendrinou-Samara, *Dalton Trans.*, 2014, **43**, 12754–12765.
26 E. Pöselt, H. Kloust, U. Tromsdorf, M. Janschel, C. Hahn, C. Maßlo and H. Weller, *ACS Nano*, 2012, **6**, 1619–1624.
27 R. De Palma, S. Peeters, M. J. Van Bael, H. Van den Rul, K. Bonroy, W. Laureyn, J. Mullens, G. Borghs and G. Maes, *Chem. Mater.*, 2007, **19**, 1821–1831.
28 G. Bokias, A. Durand and D. Hourdet, *Macromol. Chem. Phys.*, 1998, **199**, 1387–1392.
29 B. H. Tan, P. Ravi and K. C. Tam, *Macromol. Rapid Commun.*, 2006, **27**, 522–528.
30 Z. Wang, B. H. Tan, H. Hussain and C. He, *Colloid Polym. Sci.*, 2013, **291**, 1803–1815.
31 Q. L. Vuong, P. Gillis and Y. Gossuin, *J. Magn. Reson.*, 2011, **212**, 139–148.
32 H. Yang, H. Zhou, C. Zhang, X. Li, H. Hu, H. Wu and S. Yang, *Dalton Trans.*, 2011, **40**, 3616–3621.
33 M. Rohrer, H. Bauer, J. Mintorovitch, M. Requardt and H.-J. Weinmann, *Invest. Radiol.*, 2005, **40**, 715–724.